Shell corrections of superheavy nuclei in self-consistent calculations

A. T. Kruppa,[1,2] M. Bender,[3,4,5] W. Nazarewicz,[3,5,6] P.-G. Reinhard,[1,7] T. Vertse,[1,2] and S. Ćwiok[8]

[1]*Joint Institute for Heavy Ion Research, Oak Ridge National Laboratory, P.O. Box 2008, Oak Ridge, Tennessee 37831*

[2]*Institute of Nuclear Research of the Hungarian Academy of Sciences, H-4001 Debrecen, Pf. 51, Hungary*

[3]*Department of Physics and Astronomy, University of Tennessee, Knoxville, Tennessee 37996*

[4]*Department of Physics and Astronomy, University of North Carolina, Chapel Hill, North Carolina 27599*

[5]*Physics Division, Oak Ridge National Laboratory, P.O. Box 2008, Oak Ridge, Tennessee 37831*

[6]*Institute of Theoretical Physics, Warsaw University, ul. Hoża 69, PL-00681, Warsaw, Poland*

[7]*Institut für Theoretische Physik II, Universität Erlangen Staudtstr. 7, D-91058 Erlangen, Germany*

[8]*Faculty of Physics, Warsaw University of Technology, ul. Koszykowa 75, PL-00662, Warsaw, Poland*

Shell corrections to the nuclear binding energy as a measure of shell effects in superheavy nuclei are studied within the self-consistent Skyrme-Hartree-Fock and relativistic mean-field theories. As a result of the presence of a low-lying proton continuum resulting in a free particle gas, special attention is paid to the treatment of the single-particle level density. To cure the pathological behavior of the shell correction around the particle threshold, a method based on the Green's function approach has been adopted. It is demonstrated that for the vast majority of Skyrme interactions commonly employed in nuclear structure calculations, the strongest shell stabilization appears for $Z=124$ and 126, and for $N=184$. On the other hand, in the relativistic approaches the strongest spherical shell effect appears systematically for $Z=120$ and $N=172$. This difference probably has its roots in the spin-orbit potential. We have also shown that, in contrast to shell corrections which are fairly independent of the force, macroscopic energies extracted from self-consistent calculations strongly depend on the actual force parametrization used. That is, the A and Z dependence of the mass surface when extrapolating to unknown superheavy nuclei is prone to significant theoretical uncertainties.

PACS number(s): 21.10.Dr, 21.10.Pc, 21.60.Jz, 27.90.+b

I. INTRODUCTION

The stability of the heaviest and superheavy elements has been a long-standing fundamental question in nuclear science. Theoretically, the mere existence of the heaviest elements with $Z>104$ is entirely due to quantal shell effects. Indeed, for these nuclei the shape of the classical nuclear droplet, governed by surface tension and Coulomb repulsion, is unstable to surface distortions, driving these nuclei to spontaneous fission. That is, if the heaviest nuclei were governed by the classical liquid drop model, they would fission immediately from their ground states due to the large electric charge. However, in the mid-1960s, with the invention of the shell-correction method, it was realized that long-lived superheavy elements (SHEs) with very large atomic numbers could exist due to the strong shell stabilization [1–4].

In spite of tremendous experimental effort, after about 30 years of the quest for superheavy elements, the borders of the upper-right end of the nuclear chart are still unknown [5]. However, it has to be emphasized that the recent years also brought significant progress in the production of the heaviest nuclei [5,6]. During 1995–1996, three new elements, $Z=110$, 111, and 112, were synthesized by means of both cold and hot fusion reactions [7–10]. These heaviest isotopes decay predominantly by groups of α particles (α chains) as expected theoretically [11–13]. Recently, two stunning discoveries have been made. First, hot fusion experiments performed in Dubna employing ^{48}Ca$+^{244}$Pu and ^{48}Ca$+^{242}$Pu ''hot fusion'' reactions [14] gave evidence for the synthesis of two isotopes ($A=287$ and 289) of the element $Z=114$. Second, the Berkeley-Oregon team, utilizing the ''cold fu-

sion'' reaction ^{86}Kr$+^{208}$Pb [15], observed three α-decay chains attributed to the decay of the new element $Z=118$, $A=293$. The measured α-decay chains ^{289}114 and ^{293}118 turned out to be consistent with predictions of Skyrme-Hartree-Fock (SHF) theory [16] and relativistic mean-field (RMF) theory [17].

The goal of the present work is to study shell closures in SHEs. To that end we use as a tool microscopic shell corrections extracted from self-consistent calculations. For medium-mass and heavy nuclei, self-consistent mean-field theory is a very useful starting point [18]. Nowadays, SHF and RMF calculations with realistic effective forces are able to describe global nuclear properties with an accuracy which is comparable to that obtained in more phenomenological macroscopic-microscopic models based on the shell-correction method.

In previous work [19], shell energies for SHEs were extracted by subtracting from calculated HF binding energies the macroscopic Yukawa-plus-exponential mass formula [20] with the parameters of Ref. [21]. In another work, based on RMF theory [22], shell corrections were extracted for the heaviest deformed nuclei using the standard Strutinsky method in which the positive-energy spectrum was approximated by quasibound states. Neither procedure can be considered as satisfactory. A proper treatment of continuum states is achieved with a Green's-function method [23]. We employ this method for the present study of the shell corrections of SHEs.

The material contained in this study is organized as follows. The motivation of this work is outlined in Sec. II. Section III contains a brief discussion of the Strutinsky en-
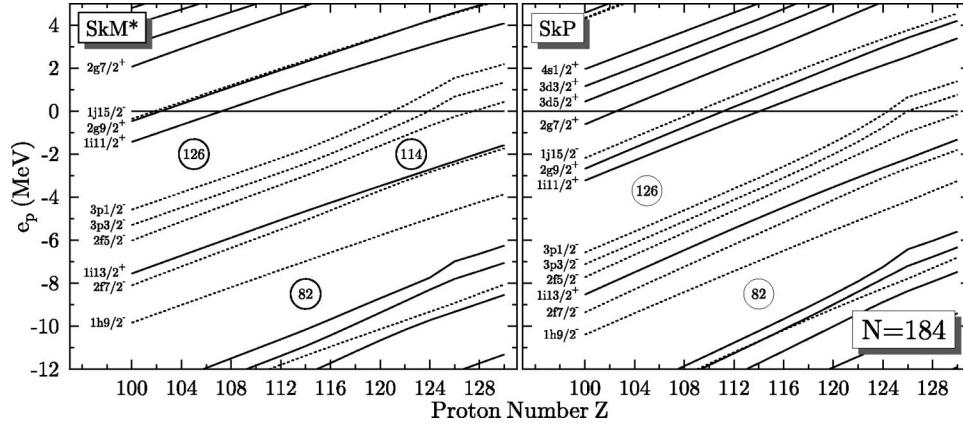
FIG. 1. Single-proton levels for $N=184$ isotones with $110 \leqslant Z \leqslant 130$ calculated in the Skyrme-Hartree-Fock model with SkM* (left) and SkP effective interactions. Positive (negative) parity levels are indicated by solid (dashed) lines and by their spherical labels (nlj). Note that in both cases the nucleus $Z=126$ is proton unbound; i.e., the $p_{1/2}$ shell has positive energy.

ergy theorem on which the concept of the shell correction is based. The Green's-function HF method used to extract the single-particle level density is presented in Sec. IV. Section V discusses the details of our HF and RMF models and describes the Strutinsky procedure employed. The results of calculations for shell corrections in spherical SHEs and for macroscopic energies extracted from self-consistent binding energies are discussed in Sec. VI. Finally, Sec. VII contains the main conclusions of this work.

II. MOTIVATION

All the heaviest elements found recently are believed to be well deformed. Indeed, the measured α-decay energies, along with complementary syntheses of new neutron-rich isotopes of elements $Z=106$ and $Z=108$, have furnished confirmation of the special stability of the deformed shell at $N=162$ predicted by theory [24,25]. Beautiful experimental confirmation of large quadrupole deformations in this mass region comes from gamma-ray spectroscopy. Recent experimental works [26,27] succeeded in identifying the ground-state band of ^{254}No (the heaviest nucleus studied in gamma-ray spectroscopy so far). The quadrupole deformation of ^{254}No, inferred from the energy of the deduced 2^+ state, is in nice agreement with theoretical predictions [19,21,28,29]. Still heavier and more neutron-rich elements are expected to be spherical due to the proximity of the neutron shell at $N=184$. This is the region of SHEs which we will investigate here.

In spite of an impressive agreement with available experimental data for the heaviest elements, theoretical uncertainties are large when extrapolating to unknown nuclei with greater atomic numbers. As discussed in Refs. [19,30], the main factors that influence the single-proton shell structure of SHEs are (i) the Coulomb potential and (ii) the spin-orbit splitting. As far as the protons are concerned, the important spherical shells are the closely spaced $1i_{13/2}$ and $2f_{7/2}$ levels which appear just below the $Z=114$ gap, the $2f_{5/2}$ shell which becomes occupied at $Z=120$, the $3p_{3/2}$ shell which becomes occupied at $Z=124$, and the $3p_{1/2}$ and $1i_{11/2}$ orbitals whose splitting determines the size of the $Z=126$ magic

gap. Interestingly, while the *ordering* of single-proton states is practically the same for all the self-consistent approaches with realistic effective interactions (see Fig. 1 and single-particle diagrams in Refs. [19,30]), their relative positions vary depending on the choice of force parameters. Since in the region of SHEs the single-particle level density is relatively large, small shifts in positions of single-particle levels can influence the strength of single-particle gaps and be crucial for determining the shell stability of a nucleus. As a result, there is no consensus between theorists concerning the next proton magic gap beyond $Z=82$. While most macroscopic-microscopic (non-self-consistent) approaches predict $Z=114$ to be magic, self-consistent calculations suggest that the center of the proton shell stability should be moved up to higher proton numbers, $Z=120$, 124, or 126 [19,29–31]. It is to be noted that the Coulomb potential mainly influences the magnitude of the $Z=114$ gap. (Here, the self-consistent treatment of the Coulomb energy is a key factor.) On the other hand, the spin-orbit interaction determines the position of the $2f$ and $3p$ shells which define the proton shell structure above $Z>114$.

The spherical neutron shell structure is governed by the following orbitals: $1j_{15/2}$ (below the $N=164$ gap), $2g_{7/2}$, $3d_{5/2}$, $3d_{3/2}$, $4s_{1/2}$, and $1j_{13/2}$ whose splitting determines the size of the $N=184$ spherical gap (see Fig. 2 and Refs. [19,30]). Again, similar to the proton case, the order of the single-neutron orbitals between $N=164$ and 184 is rather robust, while the sizes of single-particle gaps vary. For instance, the $N=172$ gap, predicted by the RMF calculations shown in Fig. 2, results from the large energy splitting between the $2g_{7/2}$ and $3d_{5/2}$ shells. In nonrelativistic models, these two orbitals are very close in energy, and this degeneracy is related to the pseudospin symmetry [32,33]. Interestingly, in the SHF calculations, the pseudospin degeneracy holds in most cases. Namely, certain neutron orbitals group in pairs (pseudospin doublets), $(2g_{7/2},3d_{5/2}),(3d_{3/2},4s_{1/2})$, and the same holds for proton orbitals, e.g., $(2f_{5/2},3p_{3/2})$. Considering the fact that the idea of pseudospin has relativistic roots [34,35], it is surprising to see that this symmetry is so dramatically violated in RMF theory. As a matter of fact,
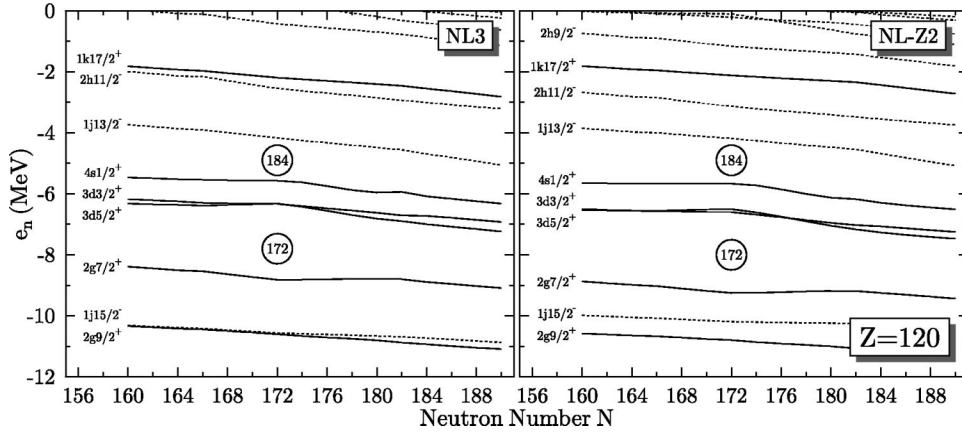
FIG. 2. Single-neutron levels for $Z=120$ isotopes with $160 \leqslant N \leqslant 190$ calculated in the RMF approach with NL3 (left) and NL-Z2 nonlinear parametrizations. The line convention is the same as in Fig. 1. Note the large neutron gaps at $N=172$ and 184.

the presence of pronounced magic gaps at $Z=120$ and $N=172$ in RMF models (see below) is a direct manifestation of the pseudospin symmetry breaking.

As discussed in Ref. [19], neutron-deficient superheavy nuclei are expected to be unstable to proton emission. Indeed, as seen in Fig. 1, the proton $3p_{1/2}$ shell has positive energy for $Z \geqslant 126$; i.e., in these nuclei the $3p_{1/2}$ level is a narrow resonance. As a result of huge Coulomb barriers, superheavy nuclei with $Q_p < 1.5$ MeV are practically proton stable [19]. However, the higher-lying single-proton orbitals are expected to have sizable proton widths.

In order to assess the magnitude of shell effects determined by the bunchiness of single-particle levels, it is useful to apply the Strutinsky renormalization procedure [36–38] which makes it possible to calculate the shell-correction energy. Unfortunately, the standard way of extracting the shell correction breaks down for weakly bound nuclei where the contribution from the particle continuum becomes important [39]. Recently, a new method of calculating the shell correction, based on the correct treatment of resonances, has been developed [40,41]. The improved method is based on the theory of Gamow states (eigenstates of a one-body Hamiltonian with purely outgoing boundary conditions) which can be calculated numerically for commonly used optical-model potentials [42]. While this "exact" procedure cannot be easily adapted to the case of microscopic self-consistent potentials, its simplified version applying the Green's-function method can [23].

III. SHELL CORRECTION AND THE ENERGY THEOREM

The main assumption of the shell-correction (macroscopic-microscopic) method [36–38,43] is that the total energy of a nucleus can be decomposed into two parts:

$$E = \widetilde{E} + E_{\text{shell}}, \tag{1}$$

where $\widetilde{E}$ is the macroscopic energy (smoothly depending on the number of nucleons and thus associated with the "uniform" distribution of single-particle orbitals) and E_{shell} is the

shell-correction term that fluctuates with particle number reflecting the nonuniformities (bunchiness) of the single-particle level distribution. In order to make a separation (1), one starts from the one-body HF density matrix ρ,

$$\rho(\mathbf{r}',\mathbf{r}) = \sum_i n_i \phi_i(\mathbf{r}') \phi_i^*(\mathbf{r}), \tag{2}$$

which can be decomposed into a "smoothed" density $\widetilde{\rho}$ and a correction $\delta\rho$, which fluctuates with the shell filling:

$$\rho = \widetilde{\rho} + \delta\rho. \tag{3}$$

In Eq. (2), n_i is the single-particle occupation coefficient which is equal to 1 (0) if the level e_i is occupied (empty). The smoothed single-particle density $\widetilde{\rho}$ can be expressed by means of the smoothed distribution numbers $\widetilde{n}_i$ [44]:

$$\widetilde{\rho}(\mathbf{r}',\mathbf{r}) = \sum_i \widetilde{n}_i \phi_i(\mathbf{r}') \phi_i^*(\mathbf{r}). \tag{4}$$

When considered as a function of the single-particle energies e_i, the numbers $\widetilde{n}_i$ vary smoothly in an energy interval of the order of the energy difference between major shells. The averaged HF Hamiltonian $\widetilde{h}_{\text{HF}}$ can be directly obtained from $\widetilde{\rho}$. The expectation value of a HF Hamiltonian (containing the kinetic energy t and the two-body interaction $\bar{v}$) can then be written in terms of $\widetilde{\rho}$ and $\delta\rho$ [43,45]:

$$E_{\text{HF}} = \text{Tr}(t\rho) + \frac{1}{2}\text{Tr Tr}(\rho\bar{v}\rho) = \widetilde{E} + E_{\text{osc}} + O(\delta\rho^2), \tag{5}$$

where

$$\widetilde{E} = \text{Tr}(t\widetilde{\rho}) + \frac{1}{2}\text{Tr Tr}(\widetilde{\rho}\bar{v}\widetilde{\rho}) \tag{6}$$

is the average part of E_{HF} and

$$E_{\text{osc}} = \text{Tr}(\widetilde{h}_{\text{HF}}\delta\rho) \quad \text{with} \quad \widetilde{h}_{\text{HF}} = t + \text{Tr}(\bar{v}\widetilde{\rho}) \tag{7}$$

is the first-order term in $\delta\rho$ representing the shell-correction contribution to E_{HF}. If a deformed phenomenological potential gives a similar spectrum to the averaged HF potential $\tilde{h}_{HF}$, then the oscillatory part of E_{HF}, given by Eq. (7), is very close to that of the deformed shell model, $E_{shell} = E_{osc} + O(\delta\rho^2)$. The second-order term in Eq. (5) is usually very small and can be neglected [46]. The above relation, known as the *Strutinsky energy theorem*, makes it possible to calculate the total energy using the non-self-consistent, deformed independent-particle model; the average part $\tilde{E}$ is usually replaced by the corresponding phenomenological liquid-drop (or droplet) model value E_{macro}. It is important that E_{shell} must not contain any regular (smooth) terms analogous to those already included in the phenomenological macroscopic part. The numerical proof of the energy theorem was carried out by Brack and Quentin [47] who demonstrated that Eq. (1) holds for E_{shell} defined by means of the smoothed single-particle energies (eigenvalues of $\tilde{h}_{HF}$).

In this work, we use a simpler expression to extract the shell correction from the HF binding energy, which should also be accurate up to $O(\delta\rho^2)$. Namely, as an input to the Strutinsky procedure we take the self-consistent single-particle HF energies e_i^{HF}. In this case, the shell correction is given by

$$E_{shell}(\rho) = \sum_i (n_i - \tilde{n}_i)e_i + O(\delta\rho^2). \tag{8}$$

The equivalent macroscopic energy can easily be computed by taking the difference

$$E_{macro} \approx \tilde{E}^{HF} = E(\rho) - E_{shell}(\rho). \tag{9}$$

IV. GREEN'S-FUNCTION HARTREE-FOCK APPROACH TO THE SHELL CORRECTION

The HF equation is generally solved using a harmonic oscillator expansion method or by means of a discretization in a three-dimensional box. In both cases, a great number of unphysical states with positive energy appear. The effect of these quasibound states is disastrous for the Strutinsky renormalization procedure [23,39–41,48]. Indeed, if one smoothes out the single-particle energy density,

$$g_{sp}(e) = \sum_i \delta(e - e_i^{HF}), \tag{10}$$

it would diverge at zero energy because of the presence of unphysical positive energy states. Consequently, the resulting shell correction becomes unreliable.

In order to avoid the divergence of $g(e)$ around the threshold, we apply the Green's-function method [23,49–52] for the calculation of the single-particle level density. In this method, the level density is given by the expression

$$g(e) = -\frac{1}{\pi} \mathrm{Im}\{\mathrm{Tr}[\hat{G}^+(e) - \hat{G}_{free}^+(e)]\}, \tag{11}$$

where $\hat{G}^+(e) = (e - \hat{h} + i0)^{-1}$ is the outgoing Green's operator of the single-particle Hamiltonian $\hat{h}(\rho)$, and $\hat{G}_{free}^+$ is the free outgoing Green's operator that belongs to the ''free'' single-particle Hamiltonian. This latter is derived from the full HF Hamiltonian in such a way that those terms are kept which are related to the kinetic energy density and to the direct Coulomb term. The interpretation of Eq. (11) is straightforward: the second term in Eq. (11) contains the contribution to the single-particle level density originating from the gas of free particles.

The single-particle level density defined by the Green's-function expression (11) behaves smoothly around the zero-energy threshold; for finite-depth Hamiltonians this definition is the only meaningful way of introducing $g(e)$. The level density (11) automatically takes into account the effect of the particle continuum which may influence the results of shell-correction calculations [40,41], especially pronounced for systems where the Fermi level is close to zero, i.e., drip-line nuclei.

Because it is difficult to calculate the Green's function, in this work we applied the approximation introduced in Ref. [23]. In this approach, the single-particle level density is expressed as

$$g(e) \approx \sum_i \delta(e - e_i^{HF}) - \sum_i \delta(e - e_i^{HF,free}), \tag{12}$$

where $e_i^{HF,free}$ are the eigenvalues of the free one-body HF Hamiltonian. As usual in the Strutinsky procedure, a smooth level density can be obtained by folding $g(e)$ with a smoothing function $f(x)$:

$$\tilde{g}(e) = \frac{1}{\gamma} \int_{-\infty}^{+\infty} de' \, g(e') f\left(\frac{e' - e}{\gamma}\right)$$

$$= \tilde{g}_0(e) - \tilde{g}_{free}(e), \tag{13}$$

where γ is the smoothing width, $\tilde{g}_0(e)$ is the smooth level density obtained from the HF spectrum (including the quasi-bound states), and $\tilde{g}_{free}(e)$ is the contribution to the smooth level density from the particle gas.

In practice, $\tilde{g}(e)$ can be calculated in three steps. First, we solve the HF equations to determine the self-consistent energies e_i^{HF}. In the next step, we calculate the positive-energy gas spectrum $e_i^{HF,free}$ *at the self-consistent minimum*. In particular, we take the Coulomb force from the self-consistent calculation. Finally, we compute $\tilde{g}_0(e)$ and $\tilde{g}_{free}(e)$ using the same folding function. The quality of approximation (12) was tested in Ref. [23] where it was demonstrated that, when increasing the number of basis states, the resulting single-particle level density quickly converges to the exact result.

V. SELF-CONSISTENT MODELS

A. Skyrme-Hartree-Fock model

In the SHF method, nucleons are described as nonrelativistic particles moving independently in a common self-consistent field. Our implementation of the HF model is

based on the standard ansatz [53]. The total binding energy of a nucleus is obtained self-consistently from the energy functional

$$\mathcal{E} = \mathcal{E}_{\mathrm{kin}} + \mathcal{E}_{\mathrm{Sk}} + \mathcal{E}_{\mathrm{Sk},ls} + \mathcal{E}_C + \mathcal{E}_{\mathrm{pair}} - \mathcal{E}_{\mathrm{c.m.}}, \qquad (14)$$

where $\mathcal{E}_{\mathrm{kin}}$ is the kinetic energy functional, $\mathcal{E}_{\mathrm{Sk}}$ is the Skyrme functional, $\mathcal{E}_{\mathrm{Sk},ls}$ is the spin-orbit functional, $\mathcal{E}_C$ is the Coulomb energy (including the exchange term), $\mathcal{E}_{\mathrm{pair}}$ is the pairing energy, and $\mathcal{E}_{\mathrm{c.m.}}$ is the center-of-mass correction.

Since there exist more than 80 different Skyrme parametrizations, the question arises, which forces should actually be used when making predictions and comparing with the data? Here, we have chosen a small subset of Skyrme forces which perform well for the basic ground-state properties (masses, radii, surface thicknesses) and have sufficiently different properties which allow one to explore the possible variations among parametrizations. This subset contains SkM* [54], SkT6 [55], Z_σ [56], SkP [57], SLy4 [58], and SkI1, SkI3, and SkI4 from Ref. [59]. We have also added the force SkO from a recent exploration [60]. Most of these interactions have been used for the investigation of the ground-state properties of SHEs before [16,19,29–31]. All the selected forces perform well concerning the total energy and radii. They all have comparable incompressibility $K = 210$–250 MeV and comparable surface energy which results from a careful fit to ground-state properties [60]. Variations occur for properties which are not fixed precisely by ground-state characteristics. The effective nucleon mass is 1 for SkT6 and SkP, 0.9 for SkO, around 0.8 for SkM* and Z_σ, and even lower, around 0.65, for SLy4, SkI1, SkI3, and SkI4. Isovector properties also exhibit large variations. For SkI3 and SkI4, the spin-orbit functional is given in the extended form of [59] which allows a separate adjustment of isoscalar and isovector spin-orbit forces. The standard Skyrme forces use the particular combination of isoscalar and isovector terms which were motivated by the derivation from a two-body zero-range spin-orbit interaction [61]. (For a detailed discussion of the spin-orbit interaction in SHF theory we refer the reader to Refs. [30,59,62–64].)

B. Relativistic mean-field model

In our implementation of the RMF model, nucleons are described as independent Dirac particles moving in local isoscalar-scalar, isoscalar-vector, and isovector-vector mean fields usually associated with σ, ω, and ρ mesons, respectively [65]. These couple to the corresponding local densities of the nucleons which are bilinear covariants of the Dirac spinors similar to the single-particle density of Eq. (2).

The RMF model is usually formulated in terms of a covariant Lagrangian; see, e.g., Ref. [65]. For our purpose we prefer a formulation in terms of an energy functional that is obtained by eliminating the mesonic degrees of freedom in the Lagrangian. For a detailed discussion of the RMF model as an energy density functional theory, see Refs. [66–69]. The energy functional of the nucleus,

$$\mathcal{E}_{\mathrm{RMF}} = \mathcal{E}_{\mathrm{kin}} + \mathcal{E}_\sigma + \mathcal{E}_\omega + \mathcal{E}_\rho + \mathcal{E}_C + \mathcal{E}_{\mathrm{pair}} - \mathcal{E}_{\mathrm{c.m.}}, \qquad (15)$$

is composed of the kinetic energy of the nucleons $\mathcal{E}_{\mathrm{kin}}$, the interaction energies of the σ, ω, and ρ fields, and the Coulomb energy of the protons $\mathcal{E}_C$. All these are bilinear in the nucleonic densities as in the case of nonrelativistic models [cf. Eq. (5)]. Pairing correlations are treated in the BCS approach employing the same nonrelativistic pairing energy functional $\mathcal{E}_{\mathrm{pair}}$ that is used in the SHF model. The center-of-mass correction $\mathcal{E}_{\mathrm{c.m.}}$ is also calculated in a nonrelativistic approximation; see [70] for a detailed discussion. The single-particle energies e_i needed to calculate the shell correction are the eigenvalues of the one-body Hamiltonian of the nucleons which is obtained by variation of the energy functional (15).

In the context of our study, it is important to note that the spin-orbit interaction emerges naturally in the RMF model from the interplay of scalar and vector fields [65]. Without any free parameters fitted to single-particle data, the RMF model gives a rather good description of spin-orbit splittings throughout the chart of nuclei [30].

As in the SHF model, there exist many RMF parametrizations which differ in details. For the purpose of the present study, we choose the most successful (or most commonly used) ones: NL1 [71], NL-Z [72], NL-Z2 [30], NL-SH [73], NL3 [74], and TM1 [75]. All of them have been used for investigations of SHEs [30,31,76,77].

The parametrization NL1 is a fit of the RMF model along the strategy of Ref. [56] used also for the Skyrme interaction Z_σ. The NL-Z parametrization is a refit of NL1 where the correction for spurious center-of-mass motion is calculated from an actual many-body wave function, while NL-Z2 is a recent variant of NL-Z with an improved isospin dependence. The force NL3 stems from a fit including exotic nuclei, neutron radii, and information on giant resonances. The NL-SH parametrization was fitted with a bias toward isotopic trends and it also uses information on neutron radii. The force TM1 was optimized in the same way as NL-SH except for introducing an additional quartic self-interaction of the isoscalar-vector field to avoid the instabilities of the standard model which occur for small nuclei. For SHEs, the results obtained with NL-Z are not distinguishable from results obtained with the parametrization PL-40, which is contained in exactly the same manner as NL-Z but uses a stabilized nonlinearity of the scalar-isoscalar field [78]. (PL-40 was employed in some recent investigations of the properties of superheavy nuclei [29,31,79].)

All the above parametrizations provide a good description of the binding energies, charge radii, and surface thicknesses of stable spherical nuclei with the same overall quality as the SHF model. The nuclear matter properties of the RMF forces, however, show some systematic differences as compared to Skyrme forces. All RMF forces have comparable small effective masses around $m^*/m \approx 0.6$. (Note that the effective mass in the RMF model depends on momentum; hence the effective mass at the Fermi energy is approximately 10% larger.) Compared with the SHF model, the absolute value of the energy per nucleon is systematically larger, with values around -16.3 MeV, while the saturation density is always slightly smaller, with typical values around 0.15 nucleons/fm^3. The compressibility of the RMF forces

ranges from low values around 170 MeV for NL-Z to $K = 355$ MeV for NL-SH, which is rather high. There are also differences in isovector properties; the symmetry energy coefficient of all RMF forces is systematically larger than for SHF interactions, with values between 36.1 MeV for NL-SH and 43.5 MeV for NL1 (see discussion below).

C. Details of the calculations

In order to probe the single-particle shell structure of SHEs, SHF, and RMF calculations were carried out under the assumption of spherical geometry. By doing so we intentionally disregard deformation effects which make it difficult to compare different models and parametrizations. For the same reason, pairing correlations were practically neglected. (In order to obtain self-consistent spherical solutions for open-shell nuclei, small constant pairing gaps $\Delta < 100$ keV were assumed; the corresponding pairing energies are negligible. This procedure is approximately equivalent to the filling approximation.)

The SHF calculations were carried out using the coordinate-space Hartree-Fock code of Ref. [80]. The HF equations were solved by the discretization method. To obtain a proper description of quasibound states, it was necessary to take a very large box and a very dense mesh. The actual box size was chosen to be 21 fm and the mesh spacing was 0.3 fm. With this choice, the low-lying positive-energy proton states obtained in the SHF model perfectly reproduce proton resonances obtained by solving the Schrödinger equation for the HF potential with purely outgoing boundary conditions.

The Strutinsky procedure contains two free parameters, the smoothing parameter γ and the order of the curvature correction p. In calculating the Strutinsky smooth energy, instead of the traditional plateau condition we applied the generalized plateau condition described in Ref. [41]. The optimal values of γ (in units of oscillator frequency $\hbar\omega_0 = 41/A^{1/3}$) calculated for several nuclei turned out to be close to $\gamma_p = 1.54$ and $\gamma_n = 1.66$ for protons and neutrons, respectively; these values, together with $p = 10$, were adopted in our calculations of shell corrections in the SHF model.

In the RMF approach, the shell correction can be extracted from the single-particle spectrum like in the SHF model. To demonstrate it, one proceeds along the steps discussed in Sec. III. The total RMF energy (15) can be decomposed into a smooth part and a correction that fluctuates according to the actual level density. Since the RMF energy functional is bilinear in the densities, the extracted shell correction should be accurate up to order $O(\delta\rho^2)$.

The RMF calculations were carried out using the coordinate-space code of Ref. [81]. As in the SHF case, the box size was chosen to be 21 fm with a mesh spacing of 0.3 fm.

As already mentioned, all successful RMF parametrizations give a rather small effective mass. This leads to a small level density around the Fermi surface which in turn requires a very large smoothing range γ when calculating the smoothed level density $\tilde{g}$. The values for γ are strongly correlated with the order of the curvature-correction polynomial p [41]; the value $p = 10$ chosen here is large enough to provide in nearly all cases a sufficiently smooth $\tilde{g}$, but also small enough that we can restrict the model space to levels up to 60 MeV, which is much larger than the space used in usual RMF calculations. We have adjusted the smoothing range γ to the actual level density of a large number of nuclei to fulfill a generalized plateau condition along the strategy of [41]. This leads always to values around $\gamma_p = 2.0$ for protons and $\gamma_n = 2.2$ for neutrons. All results presented in this paper are calculated with $p = 10$ and γ fixed at these values.

VI. RESULTS

A. Spherical shell corrections in superheavy nuclei

According to the SHF calculations of Ref. [19], the spherical magic neutron number in the SHE region is $N = 184$; all the $N = 184$ isotones have been predicted to have spherical shapes. The magicity of $N = 184$ in the SHF model is confirmed in this study. Figure 3 displays the neutron shell correction calculated in several SHF models as a function of N for $Z = 120$. The absolute minimum of the shell energy always appears at $N = 184$. The $N = 172$ shell effect is also seen, but it exhibits a strong force dependence (it is particularly pronounced for Z_σ, SkI3, SkI4, and SLy4).

As already mentioned, the neutron levels have the same ordering for nearly all forces; all differences seen in the shell corrections are therefore caused by slight changes in the relative distances of the single-particle levels between the models. Forces with large effective masses like SkO, SkP, and SkT6 give a comparatively large level density which washes out the shell effects below $N = 184$. Forces with small effective masses (i.e., smaller level density) are much more likely to show significant shell effects at lower neutron numbers around $N = 172$.

At fixed Z, the proton shell correction changes rather gradually as a function of neutron number; this is illustrated in Fig. 3 for the Skyrme force SkM*. (Most of the Skyrme forces give a similar result.) Note that the proton shell corrections are generally smaller than those for the neutrons. At a second glance, however, one sees that the slow variations of the proton shell correction with neutron number are correlated with neutron shell closures. For instance, the $Z = 120$ shell correction is largest at neutron numbers around $N = 172$ and it becomes reduced when approaching $N = 184$. This is caused by the self-consistent rearrangement of single-particle levels according to the actual density distribution in the nucleus and cannot appear in macroscopic-microscopic models with assumed average potentials (see Refs. [30,31] for more discussion related to this point).

Proton shell corrections for the $N = 184$ and $N = 172$ isotones, obtained in the SHF model, are displayed in Fig. 4 as a function of Z. For SkM*, neutron shell corrections are also shown for the $N = 172$ and $N = 184$ isotones. The shift of the magic proton number with neutron number when going from $N = 172$ to $N = 184$ is clearly visible. For $N = 172$ most of the Skyrme forces (exceptions are SkT6 and SkP) agree on a magic $Z = 120$, while for $N = 184$ the shell correction shows
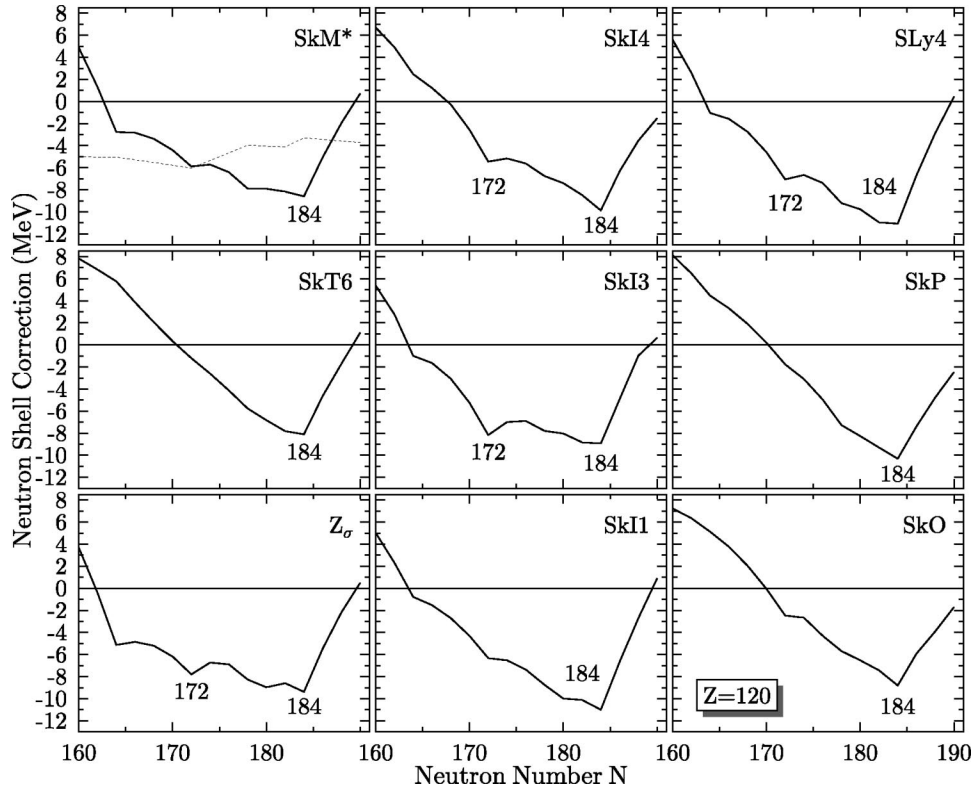
FIG. 3. Spherical neutron shell corrections for the $Z=120$ isotopes calculated in nine Skyrme-Hartree-Fock models. The dotted line for SkM* shows the proton shell correction for comparison. In all nine cases, the minimum of the shell correction is predicted at $N=184$.

a minimum at $Z=124–126$ in all cases. (Actually, in most cases, shell corrections slightly favor $Z=124$ over $Z=126$; this is related to the gradual increase of the single-particle energies of $3p_{3/2}$ and $3p_{1/2}$ orbitals above $Z=120$.)

Proton shell corrections and the $N=172$ neutron shell corrections are systematically smaller than those for neutrons at $N=184$. This partly explains why spherical ground states of SHEs are so well correlated with the magic neutron number $N=184$; see, e.g., [19,22,29]. Note that for the majority of Skyrme forces the $N=172$ isotones are predicted to be deformed.

Skyrme forces with nonstandard isospin dependence of the spin-orbit interaction are the only ones that give additional (but not very pronounced) shell closures. In the SkI4 model, there appears a secondary minimum at $Z=114$ for $N=184$, while SkI3 is the only Skyrme force which points at $Z=120$ also for $N=184$. A nonstandard spin-orbit interaction, however, does not neccesarily lead to shell closures other than $Z=124–126$ for $N=184$. For SkO, which has a spin-orbit force that is similar to SkI4, the $Z=114$ shell is only hinted. It is to be noted that for several interactions, such as Z_σ, SkIx, and SkO, the shell correction changes rather slowly between $Z=114$ and $Z=126$. This indicates that none of the proton shell gaps in this region can be considered as truly ''magic.'' (The weak Z dependence of the proton shell correction above $Z=114$ was pointed out in the early reference [82].)

The RMF results presented in Figs. 5 and 6 show a pattern that is internally consistent but different from that of SHF theory. The minimum of the neutron shell correction is sys-

tematically predicted at $N=172$. Except for NL-SH and TM1, the shell effect at $N=182–184$ is also clearly seen. Note that the $N=184$ gap in the single-particle spectrum is in all cases larger than the one at $N=182$ (see Fig. 2). The gaps are separated by a single $4s_{1/2}$ level which contributes very weakly to the shell energy. To illustrate the variation of proton shell effects along the $Z=120$ chain, proton shell corrections in NL-Z2 are also displayed in Fig. 5. Their pattern is very similar to that obtained in SHF models.

Looking at the proton shell corrections along the chain of $N=184$ isotones (see Fig. 6), the strongest shell effect is now obtained for $Z=120$. When comparing the results for the $N=184$ and $N=172$ chains, it can be seen again that the proton shell correction at $Z=120$ is strongly correlated with neutron number $N=172$. However, unlike in SHF theory, the $Z=120$ shell does not vanish completely for $N=184$. Proton shell corrections obtained with NL1, NL-Z, and NL-Z2 at $N=184$ vary rather slowly between $Z=120$ and $Z=126$, and this resembles the pattern obtained in SHF theory. Again, as in the case of Skyrme forces, proton shell corrections in RMF theory are smaller than those for the neutrons (cf. NL-Z2 calculations in Fig. 6). The increase in the proton shell correction at very large values of Z for TM1 is related to the spherical $Z=132$ shell predicted by this interaction [31].

Shell closures can also be analyzed in terms of the two-neutron and two-proton shell gaps

$$\delta_{2n}=E(N+2,Z)-2E(N,Z)+E(N-2,Z),$$
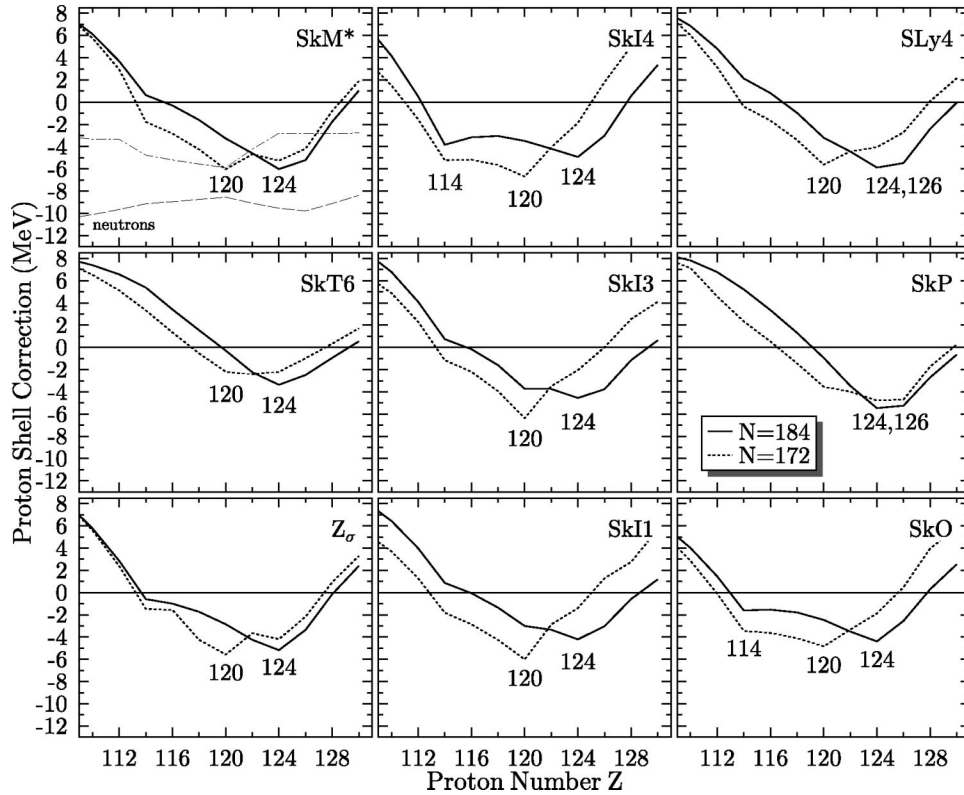
$$\delta_{2p}=E(N,Z+2)-2E(N,Z)+E(N,Z-2), \quad (16)$$

FIG. 4. Spherical proton shell corrections for the chains of $N=184$ isotones (solid lines) and $N=172$ isotones (dotted lines) calculated in nine Skyrme-Hartree-Fock models. The dashed (dash-dotted) line for SkM* shows the neutron shell correction for $N=184$ ($N=172$). For $N=184$, the minimum of the shell correction is predicted at $Z=124-126$ for all parametrizations.

discussed in Refs. [31,77]. The pattern of shell corrections calculated in SHF and RMF models qualitatively resembles the behavior of neutron and proton shell gaps found there. In particular, the strong correlation between shell effects at $Z=120$ and $N=172$ in the RMF model is seen in both representations. (It should be emphasized, however, that two-

proton shell gaps and shell corrections are not equivalent and a quantitative comparison between these quantities cannot be made.) While shell gaps are related (but not equivalent) to the gaps in the single-particle spectrum, the shell correction gives also a measure of the stabilizing effect of a shell closure on the nuclear binding energy.
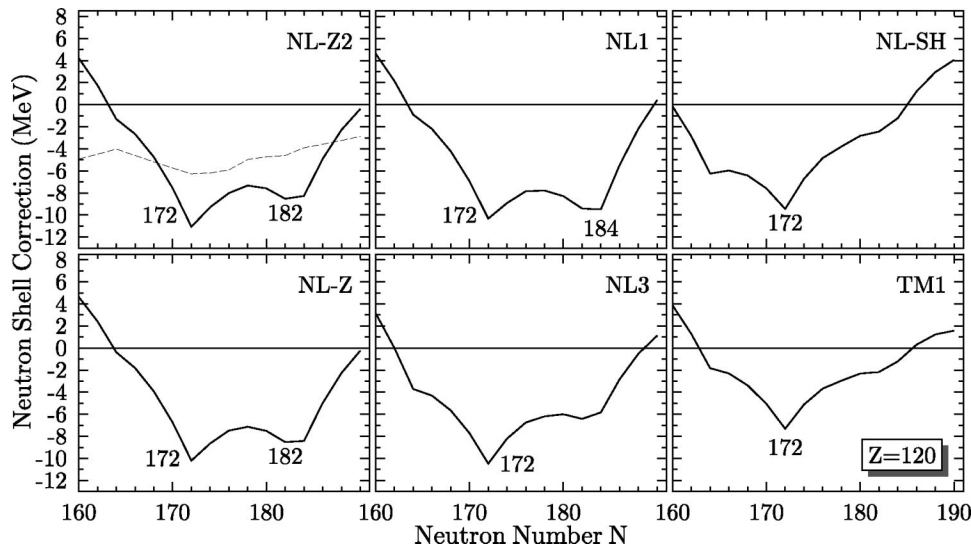

FIG. 5. Spherical neutron shell corrections for the $Z=120$ isotopes calculated in six relativistic mean-field models. In all six cases, the minimum of the shell correction is predicted at $N=172$. For NL-Z2 the proton shell correction is given for comparison by the dashed line.
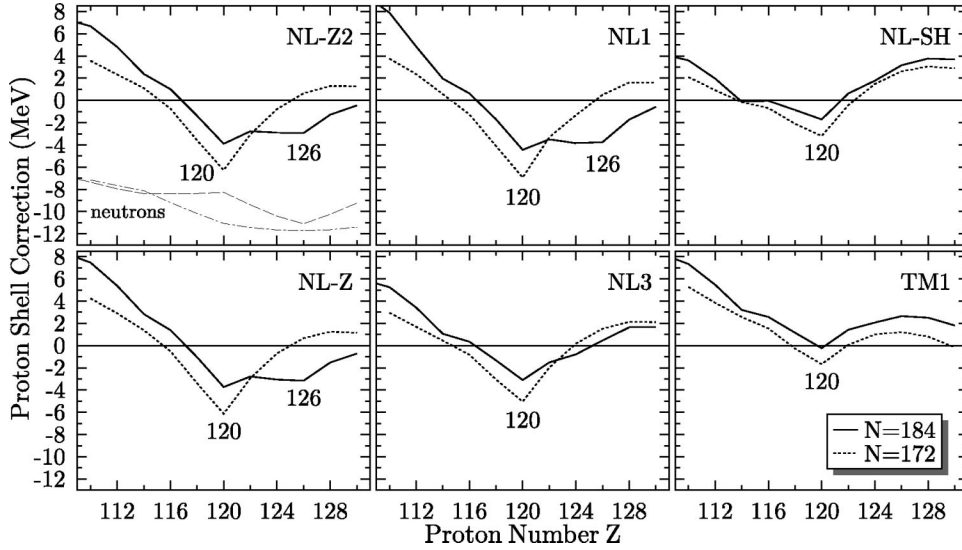
FIG. 6. Spherical proton shell corrections for the $N=184$ (solid line) and $N=172$ (dotted line) isotones calculated in six relativistic mean-field models. For all parametrizations, the minimum of the proton shell correction is predicted at $Z=120$. For NL-Z2 the neutron shell corrections for the $N=184$ (dashed line) and $N=172$ (dash-dotted line) isotones are given for comparison.

B. Macroscopic energies

By subtracting the shell correction from the calculated binding energy, one obtains a rough estimate for the associated macroscopic energy E_{macro}, Eq. (9). The macroscopic part of the SHF and RMF energies for the $N=184$ isotones as a function of Z is displayed in Fig. 7. The macroscopic energy of the Yukawa-plus-exponential mass formula of the finite-range liquid-drop model (FRLDM) of Ref. [20], with parameters of Ref. [21], is also shown for comparison. To illustrate the Z dependence, all energies were normalized to the value at $Z=100$. In general, the behavior of E_{macro} is similar in all cases. In particular, the macroscopic proton drip line is consistently predicted to be at $Z\approx120$–124. It is interesting to note that the only Skyrme force which agrees with the FRLDM is SLy4; other forces deviate from it sig-

nificantly. The RMF forces give qualitatively the same results; there are several forces (NL-Z, TM1, and NL-SH) which give values of E_{macro} close to the FRLDM.

In an attempt to understand the pattern shown in Fig. 7, we employed the simple liquid-drop model expression

$$E_{\text{macro,LDM}}=a_{\text{vol}}A+a_{\text{surf}}A^{2/3}+a_{\text{sym}}\frac{(N-Z)^2}{A}+a_{\text{Coul}}\frac{Z^2}{A^{1/3}}. \tag{17}$$

The parameters a_i of Skyrme and RMF forces were calculated in the limit of symmetric nuclear matter; they are given in Table I, together with the values for the standard liquid-drop model (LDM) of Ref. [84]. [Note that these values change slightly when including higher-order terms in the
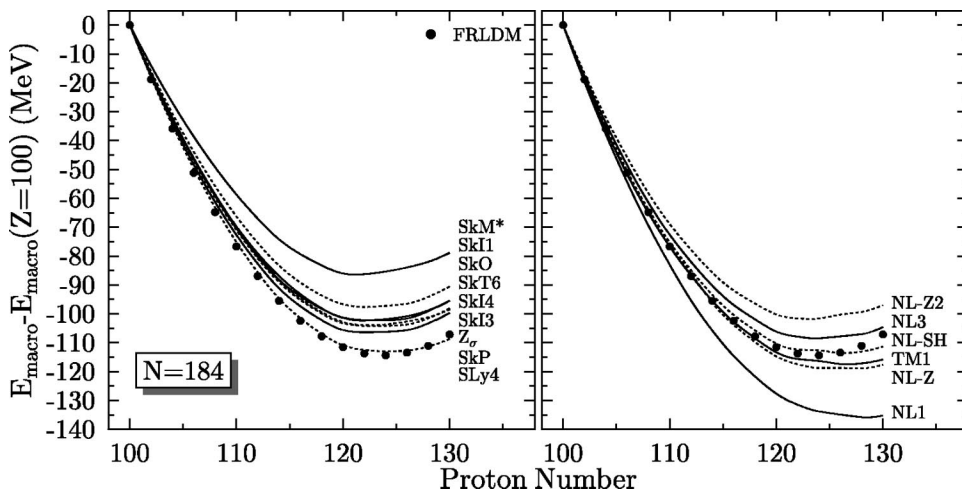

FIG. 7. Macroscopic energy $\tilde{E}^{\text{HF}}$, Eq. (9), extracted from the calculated Hartree-Fock energies of the $N=184$ isotones. For comparison, the phenomenological macroscopic energy of the Yukawa-plus-exponential mass formula (FRLDM) of Ref. [20] with parameters of Ref. [21] is also displayed. To illustrate the Z dependence, all energies were normalized to the FRLDM value at $Z=100$.

TABLE I. Key properties of symmetric nuclear matter for the Skyrme and RMF forces used in this paper: binding energy per nucleon, surface energy, and symmetry energy, all in MeV. The RMF values for a_{surf} are taken from Ref. [83]. The standard liquid-drop model (LDM) values [84] are also shown.

Force	a_{vol}	a_{surf}	a_{sym}
SkM*	-15.9	17.59	30.0
Z_σ	-15.9	16.94	26.7
SkT6	-16.1	18.12	29.9
SLy4	-16.1	18.18	32.0
SkI1	-15.9	17.31	37.5
SkI3	-16.0	17.52	34.8
SkI4	-15.9	17.28	29.5
SkP	-16.0	17.95	30.0
SkO	-15.8	17.00	32.0
NL1	-16.4	18.66	43.5
NL-Z	-16.2	17.72	41.7
NL-Z2	-16.1		39.0
NL3	-16.2	18.46	37.4
NL-SH	-16.3	19.05	36.1
TM1	-16.3		36.9
LDM	-15.7	18.56	28.1

LDM expansion (17).] Figure 8 shows the macroscopic energy (17) as a function of Z for the $N=184$ isotones. The huge differences between results for various Skyrme and RMF parametrizations can be traced back to their different symmetry-energy coefficients. Indeed, for most of the forces discussed, a_{sym} is significantly greater than that of the LDM, and this results in an increased slope of $E_{macro, LDM}$. For the RMF forces the significantly larger a_{vol} even further increases the difference with respect to the LDM. Unfortunately, there is very little similarity between the results of the microscopic calculations of Fig. 7 and the results of expansion (17). When comparing the energy scales of Figs. 7 and 8, one finds huge differences, of the order of 100 MeV, be-

tween E_{macro} and $E_{macro, LDM}$. While for the RMF model the energy ordering remains the same in both cases, this feature does not hold for the SHF model. Only when looking at $E_{macro, LDM}$ are the results ordered according to the corresponding values of a_{sym}, as expected. All this indicates that even for very heavy nuclei with $A \sim 300$, the simple leptodermous expansion with parameters taken from nuclear matter calculations is not going to work [85,86]; finite-size effects are still very important for SHEs.

In spite of the fact that macroscopic energies extracted from different self-consistent models systematically differ, the corresponding shell corrections are similar. For instance, the general pattern and magnitude of shell energies displayed in Figs. 3 and 4 do not depend very much on the Skyrme interaction used, and the same is true for the RMF results shown in Figs. 5 and 6. This means that although the global properties of the effective interactions employed in this work differ, their single-particle spectra are fairly similar. Hence, shell corrections extracted from self-consistent single-particle spectra are very useful measures of the spectral properties of effective forces. Figure 7 also illustrates how dangerous it is to extrapolate self-consistent results in the region of SHE's. The trends of relative binding energies (e.g., Q_α values) are expected to smoothly deviate from force to force. The nice agreement with experimental data for the heaviest elements obtained in the SHF calculations with SLy4 [16] and in the macroscopic-microscopic calculations with the FRLDM [21] indicates that the macroscopic energies of forces which are too far off the FRLDM values, i.e., SkM*, SkI1, and NL1, are probably not reliable in this region.

Figure 7 shows that the power of a force for predicting total binding energies is fairly independent of its predictive power for shell effects. Forces with a similar (good) description of the smooth trends of binding energies can yield rather different magic numbers; compare, e.g., SLy4 and NL3.

VII. CONCLUSIONS

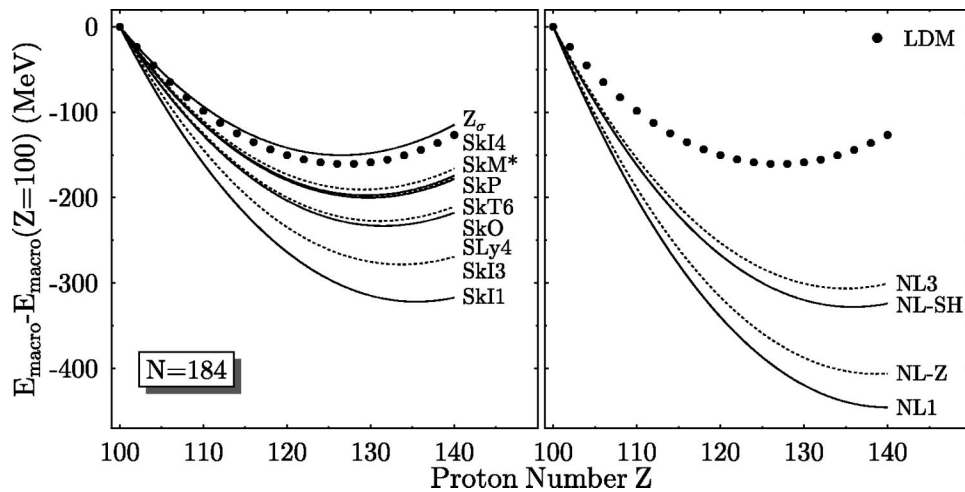The recent experimental progress in the search for new superheavy elements opens a new window for systematic

FIG. 8. Macroscopic energy $E_{macro,LDM}$, Eq. (17), for the $N=184$ isotones as a function of Z calculated for several Skyrme forces (lines) and the standard liquid-drop model (dots). To illustrate the Z dependence, all energies were normalized to zero at $Z=100$. The bulk parameters of Skyrme forces are given in Table I. The Coulomb-energy constant was assumed to be $a_{Coul}=0.717$ MeV [84] in all cases.

explorations of the limit of nuclear mass and charge. Theoretically, predictions in the region of SHEs are bound to be extrapolations from the lighter systems. An interesting and novel feature of SHEs is that the Coulomb interaction can no longer be treated as a small perturbation atop the nuclear mean field; its feedback on the nuclear potential is significant.

The main objective of this study was to perform a detailed analysis of shell effects in SHEs. Since many nuclei from this region are close to the proton drip line, a new method of calculating shell corrections, based on the Green's-function approach, had to be developed. This technique was applied to a family of Skyrme interactions and to several RMF parametrizations. This tool turned out to be extremely useful for analyzing the spectral properties of self-consistent mean fields.

It has been concluded that both the SHF and RMF calculations are *internally* consistent. That is, *all* the Skyrme models employed in this work predict the strongest spherical shell effect at $N=184$ and $Z=124,126$. On the other hand, *all* the RMF parametrizations yield the strongest shell effect at $N=172$ and $Z=120$. It is very likely that the main factor contributing to this difference is the spin-orbit interaction or, rather, its isospin dependence [30,59,62–64]. The role of the spin-orbit potential in determining the stability of SHEs was posed already in the 1970s [87,88]. The experimental determination of the center of shell stability in the region of

SHEs will, therefore, be of extreme importance for pinning down the question of the spin-orbit force.

Another interesting conclusion of our work is that the pseudospin symmetry seems to be strongly violated in the RMF calculations for SHEs. As a matter of fact, the $N=172$ and $Z=120$ magic gaps predicted in the relativistic model appear as a direct consequence of pseudospin breaking. This is quite surprising in light of several recent works on the pseudospin conservation in RMF theory [35,89].

Finally, from calculated masses we extracted self-consistent macroscopic energies. They show a significant spread when extrapolating to unknown SHEs. This is expected to give rise to systematic (smooth) deviations between masses and mass differences obtained in various self-consistent models.

ACKNOWLEDGMENTS

[1] W.D. Myers and W.J. Swiatecki, Nucl. Phys. **81**, 1 (1966).

[2] A. Sobiczewski, F.A. Gareev, and B.N. Kalinkin, Phys. Lett. **22**, 500 (1966).

[3] H. Meldner, Ark. Fys. **36**, 593 (1967).

[4] U. Mosel and W. Greiner, Z. Phys. **222**, 261 (1969).

[5] S. Hofmann and G. Münzenberg, Rev. Mod. Phys. (submitted).

[6] S. Hofmann, Nucl. Phys. **A616**, 370c (1997).

[7] S. Hofmann, V. Ninov, F.P. Hessberger, P. Armbruster, H. Folger, G. Münzenberg, H.J. Schött, A.G. Popeko, A.V. Yeremin, A.N. Andreyev, S. Saro, R. Janik, and M. Leino, Z. Phys. A **350**, 277 (1995); **350**, 281 (1995).

[8] A. Ghiorso, D. Lee, L.P. Somerville, W. Loveland, J.M. Nitschke, W. Ghiorso, G.T. Seaborg, P. Wilmarth, R. Leres, A. Wydler, M. Nurmia, K. Gregorich, R. Gaylord, T. Hamilton, N.J. Hannink, D.C. Hoffman, C. Jarzynski, C. Kacher, B. Kadkhodayan, S. Kreek, M. Lane, A. Lyon, M.A. McMahan, M. Neu, T. Sikkeland, W.J. Swiatecki, A. Türler, J.T. Walton, and S. Yashita, Nucl. Phys. **A583**, 861c (1995).

[9] Yu.A. Lazarev, Yu.V. Lobanov, Yu.Ts. Oganessian, V.K. Utyonkov, F.Sh. Abdullin, A.N. Polyakov, J. Rigol, I.V. Shirokovsky, Yu.S. Tsyganov, S. Iliev, V.G. Subbotin, A.M. Sukhov, G.V. Buklanov, B.N. Gikal, V.B. Kutner, A.N. Mezentsev, K. Subotic, J.F. Wild, R.W. Lougheed, and K.J. Moody, Phys. Rev. C **54**, 620 (1996).

[10] S. Hofmann, V. Ninov, F.P. Hessberger, P. Armbruster, H. Folger, G. Münzenberg, H.J. Schött, A.G. Popeko, A.V. Yeremin, S. Saro, R. Janik, and M. Leino, Z. Phys. A **354**, 229 (1996).

[11] S. Ćwiok and A. Sobiczewski, Z. Phys. A **342**, 203 (1992).

[12] R. Smolańczuk, Phys. Rev. C **56**, 812 (1997).

[13] R. Smolańczuk, Phys. Rev. C **60**, 021301 (1999).

[14] Yu.Ts. Oganessian, A.V. Yeremin, A.G. Popeko, S.L. Bogomolov, G.V. Buklanov, M.L. Chelnokov, V.I. Chepigin, B.N. Gikal, V.A. Gorshkov, G.G. Gulbekian, M.G. Itkis, A.P. Kabachenko, A.Yu. Lavrentev, O.N. Malyshev, J. Rohac, R.N. Sagaidak, S. Hofmann, S. Saro, G. Giargina, and K. Morita, Nature (London) **400**, 242 (1999).

[15] V. Ninov, K.E. Gregorich, W. Loveland, A. Ghiorso, D.C. Hoffman, D.M. Lee, H. Nitsche, W.J. Swiatecki, U.W. Kirbach, C.A. Laue, J.L. Adams, J.B. Patin, D.A. Shaughnessy, D.A. Strellis, and P.A. Wilk, Phys. Rev. Lett. **83**, 1104 (1999).

[16] S. Ćwiok, P.-H. Heenen, and W. Nazarewicz, Phys. Rev. Lett. **83**, 1108 (1999).

[17] M. Bender, Phys. Rev. C **61**, 031302 (2000).

[18] S. Åberg, H. Flocard, and W. Nazarewicz, Annu. Rev. Nucl. Part. Sci. **40**, 439 (1990).

[19] S. Ćwiok, J. Dobaczewski, P.-H. Heenen, P. Magierski, and W. Nazarewicz, Nucl. Phys. **A611**, 211 (1996).

[20] P. Möller and J.R. Nix, At. Data Nucl. Data Tables **39**, 213 (1988).

[21] S. Ćwiok, S. Hofmann, and W. Nazarewicz, Nucl. Phys. **A573**, 356 (1994).

[22] G.A. Lalazissis, M.M. Sharma, P. Ring, and Y.K. Gambhir, Nucl. Phys. **A608**, 202 (1996).

[23] A.T. Kruppa, Phys. Lett. B **431**, 237 (1998).

[24] S. Ćwiok, V.V. Pashkevich, J. Dudek, and W. Nazarewicz, Nucl. Phys. **A410**, 254 (1983).

[25] P. Möller and J.R. Nix, J. Phys. G **20**, 1681 (1994).

[26] P. Reiter, T.L. Khoo, C.J. Lister, D. Seweryniak, I. Ahmad, M. Alcorta, M.P. Carpenter, J.A. Cizewski, C.N. Davids, G. Gervais, J.P. Greene, W.F. Henning, R.V.F. Janssens, T. Lauritsen, S. Siem, A.A. Sonzogni, D. Sullivan, J. Uusitalo, I. Wiedenhöver, N. Amzal, P.A. Butler, A.J. Chewter, K.Y. Ding, N. Fotiades, J.D. Fox, P.T. Greenlees, R.-D. Herzberg, G.D. Jones, W. Korten, M. Leino, and K. Vetter, Phys. Rev. Lett. **82**, 509 (1999).

[27] M. Leino, H. Kankaanpaa, R.-D. Herzberg, A.J. Chewter, F.P. Hessberger, Y. Le Coz, F. Becker, P.A. Butler, J.F.C. Cocks, O. Dorvaux, K. Eskola, J. Gerl, P.T. Greenlees, K. Helariutta, M. Houry, G.D. Jones, P. Jones, R. Julin, S. Juutinen, H. Kettunen, T.L. Khoo, A. Kleinbohl, W. Korten, P. Kuusiniemi, R. Lucas, M. Muikku, P. Nieminen, R.D. Page, P. Rahkila, P. Reiter, A. Savelius, Ch. Schlegel, Ch. Theisen, W.H. Trzaska, and H.-J. Wollersheim, Eur. Phys. J. A **6**, 63 (1999).

[28] Z. Patyk and A. Sobiczewski, Nucl. Phys. **A533**, 132 (1991).

[29] T. Bürvenich, K. Rutz, M. Bender, P.-G. Reinhard, J.A. Maruhn, and W. Greiner, Eur. Phys. J. A **3**, 139 (1998).

[30] M. Bender, K. Rutz, P.-G. Reinhard, J.A. Maruhn, and W. Greiner, Phys. Rev. C **60**, 034304 (1999).

[31] K. Rutz, M. Bender, T. Bürvenich, T. Schilling, P.-G. Reinhard, J.A. Maruhn, and W. Greiner, Phys. Rev. C **56**, 238 (1997).

[32] A. Arima, M. Harvey, and K. Shimizu, Phys. Lett. **30B**, 517 (1969).

[33] K.T. Hecht and A. Adler, Nucl. Phys. **A137**, 129 (1969).

[34] J.N. Ginocchio, Phys. Rev. Lett. **78**, 436 (1997).

[35] J.N. Ginocchio and D.G. Madland, Phys. Rev. C **57**, 1167 (1998).

[36] V.M. Strutinsky, Nucl. Phys. **A95**, 420 (1967).

[37] V.M. Strutinsky, Nucl. Phys. **A122**, 1 (1968).

[38] M. Brack, J. Damgård, A.S. Jensen, H.C. Pauli, V.M. Strutinsky, and C.Y. Wong, Rev. Mod. Phys. **44**, 320 (1972).

[39] W. Nazarewicz, T.R. Werner, and J. Dobaczewski, Phys. Rev. C **50**, 2860 (1994).

[40] N. Sandulescu, O. Civitarese, R.J. Liotta, and T. Vertse, Phys. Rev. C **55**, 1250 (1997).

[41] T. Vertse, A.T. Kruppa, R.J. Liotta, W. Nazarewicz, N. Sandulescu, and T.R. Werner, Phys. Rev. C **57**, 3089 (1998).

[42] T. Vertse, K.F. Pál, and Z. Balogh, Comput. Phys. Commun. **27**, 309 (1982).

[43] G.G. Bunatian, V.M. Kolomietz, and V.V. Strutinsky, Nucl. Phys. **A188**, 225 (1972).

[44] M. Brack and P. Quentin, *Physics and Chemistry of Fission* (IAEA, Vienna, 1974), Vol. I, p. 231.

[45] P. Ring and P. Schuck, *The Nuclear Many-Body Problem* (Springer-Verlag, Berlin, 1980).

[46] M. Brack and P. Quentin, Nucl. Phys. **A361**, 35 (1981).

[47] M. Brack and P. Quentin, Phys. Lett. **56B**, 421 (1975).

[48] M. Bolsterli, E.O. Fiset, J.R. Nix, and J.L. Norton, Phys. Rev. C **5**, 1050 (1972).

[49] R. Balian and C. Bloch, Ann. Phys. (N.Y.) **60**, 401 (1970).

[50] R. Balian and C. Bloch, Ann. Phys. (N.Y.) **69**, 76 (1971).

[51] S. Shlomo, Nucl. Phys. **A539**, 17 (1992).

[52] S. Shlomo, V.M. Kolomietz, and H. Dejbakhsh, Phys. Rev. C **55**, 1972 (1996).

[53] P. Quentin and H. Flocard, Annu. Rev. Nucl. Part. Sci. **28**, 523 (1978).

[54] J. Bartel, P. Quentin, M. Brack, C. Guet, and H.B. Håkansson, Nucl. Phys. **A386**, 79 (1982).

[55] F. Tondeur, M. Brack, M. Farine, and J.M. Pearson, Nucl. Phys. **A420**, 297 (1984).

[56] J. Friedrich and P.-G. Reinhard, Phys. Rev. C **33**, 335 (1986).

[57] J. Dobaczewski, H. Flocard, and J. Treiner, Nucl. Phys. **A422**, 103 (1984).

[58] E. Chabanat, Ph.D. thesis, Université Claude Bernard Lyon-1, 1995, Report No. LYCEN T 9501 (unpublished).

[59] P.-G. Reinhard and H. Flocard, Nucl. Phys. **A584**, 467 (1995).

[60] P.-G. Reinhard, D.J. Dean, W. Nazarewicz, J. Dobaczewski, J.A. Maruhn, and M.R. Strayer, Phys. Rev. C **60**, 014316 (1999).

[61] D. Vautherin and D.M. Brink, Phys. Rev. C **5**, 626 (1972).

[62] M.M. Sharma, G. Lalazissis, G. König, and P. Ring, Phys. Rev. Lett. **74**, 3744 (1995).

[63] E. Chabanat, P. Bonche, P. Haensel, J. Meyer, and F. Schaeffer, Phys. Scr. **T56**, 231 (1995).

[64] M. Onsi, R.C. Nayak, J.M. Pearson, H. Freyer, and W. Stocker, Phys. Rev. C **55**, 3166 (1997).

[65] P.-G. Reinhard, Rep. Prog. Phys. **52**, 439 (1989).

[66] C. Speicher, R.M. Dreizler, and E. Engel, Ann. Phys. (N.Y.) **213**, 312 (1992).

[67] R.N. Schmid, E. Engel, and R.M. Dreizler, Phys. Rev. C **52**, 164 (1995).

[68] R.N. Schmid, E. Engel, and R.M. Dreizler, Phys. Rev. C **52**, 2804 (1995).

[69] R.N. Schmid, E. Engel, and R.M. Dreizler, Found. Phys. **27**, 1257 (1997).

[70] M. Bender, K. Rutz, P.-G. Reinhard, and J. A. Maruhn, Eur. Phys. J. A (to be published).

[71] P.-G. Reinhard, M. Rufa, J. Maruhn, W. Greiner, and J. Friedrich, Z. Phys. A **323**, 13 (1986).

[72] M. Rufa, P.-G. Reinhard, J.A. Maruhn, W. Greiner, and M.R. Strayer, Phys. Rev. C **38**, 390 (1988).

[73] M.M. Sharma, M.A. Nagarajan, and P. Ring, Phys. Lett. B **312**, 377 (1993).

[74] G.A. Lalazissis, J. König, and P. Ring, Phys. Rev. C **55**, 540 (1997).

[75] Y. Sugahara and H. Toki, Nucl. Phys. **A579**, 557 (1994).

[76] G.A. Lalazissis, M.M. Sharma, P. Ring, and Y.K. Gambhir, Nucl. Phys. **A608**, 202 (1996).

[77] M. Bender, K. Rutz, P.-G. Reinhard, J.A. Maruhn, and W. Greiner, in Proceedings of Nuclear Shapes and Motions, A Symposium in Honor of Ray Nix, Santa Fe, New Mexico, 1998 [Acta Phys. Hung. New Ser.: Heavy-Ion Phys. (to be published)].

[78] P.-G. Reinhard, Z. Phys. A **329**, 257 (1988).

[79] M. Bender, K. Rutz, P.-G. Reinhard, J.A. Maruhn, and W. Greiner, Phys. Rev. C **58**, 2126 (1998).

[80] P.-G. Reinhard, in *Computational Nuclear Physics I*, edited by K. Langanke, S.E. Koonin, and J.A. Maruhn (Springer-Verlag, Berlin, 1991), p. 28.

[81] K. Rutz, Ph.D. thesis, J.W. Goethe-Universität Frankfurt am Main, Ibidem-Verlag, Stuttgart, 1999.

[82] M. Bolsterli, E.O. Fiset, J.R. Nix, and J.L. Norton, Phys. Rev. Lett. **27**, 681 (1971).

[83] W. Stocker and T.v. Chossy, Phys. Rev. C **58**, 2777 (1998).

[84] W.D. Myers and W.J. Swiatecki, Ann. Phys. (N.Y.) **55**, 395 (1969).

[85] M. Brack, C. Guet, and H.-B. Håkansson, Phys. Rep. **123**, 275 (1985).

[86] M. Brack and R.K. Bhaduri, *Semiclassical Physics* (Addison-Wesley, Reading, MA, 1997).

[87] J.M. Moss, Phys. Rev. C **17**, 813 (1978).

[88] Y. Tanaka, Y. Oda, F. Petrovich, and R.K. Sheline, Phys. Lett. **83B**, 279 (1979).

[89] J. Meng, K. Sugawara-Tanabe, S. Yamaji, P. Ring, and A. Arima, Phys. Rev. C **58**, R628 (1998).